Applied Energy 397 (2025) 126342

Contents lists available at ScienceDirect

Applied Energy

journal homepage: www.elsevier.com/locate/apen

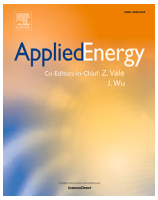

Quantification of electrical system flexibility by local multi-energy systems: Impact of the system design and component interdependencies

Philipp Glücker[a, b, c, *], Sleiman Mhanna[b], Thiemo Pesch[a], Andrea Benigni[a, c, d], Pierluigi Mancarella[b, e]

[a] Forschungszentrum Jülich GmbH, Institute of Climate and Energy Systems, ICE-1: Energy Systems Engineering, Jülich 52425, Germany
[b] Department of Electrical and Electronic Engineering, The University of Melbourne, Melbourne, Victoria 3010, Australia
[c] RWTH Aachen University, Aachen 52056, Germany
[d] JARA-Energy, Jülich 52425, Germany
[e] Department of Electrical and Electronic Engineering, The University of Manchester, M13 9PL Manchester, United Kingdom

HIGHLIGHTS

- Flexibility calculation over multiple time steps contingent on a reference schedule.
- Technical flexibility assessment of multi-energy systems embedded in the design stage.
- Heat pump combined with thermal energy storage enhances electrical flexibility potential.
- Flexibility threshold identified between thermal energy storage and heat pump.

ARTICLE INFO

Keywords:
Component sizing
Energy community
Flexibility
Heat pump
Multi-energy system
Nodal operating envelope

ABSTRACT

Multi-energy systems (MES) providing electrical flexibility will be essential for low-carbon power grids. With the aim of embedding flexibility provision into the design phase of local MES, the presented framework proposes a quantitative assessment of how the sizing of individual and interdependent components affects technical flexibility. It identifies key components that either enhance *or* reduce the flexibility of MES. The framework includes a sensitivity analysis that provides valuable technical insights, such as a deeper understanding of limiting factors and interdependencies between components across energy vectors. Moreover, flexibility is quantified over multiple time steps in relation to a predetermined reference schedule, which is particularly important for energy systems that must submit their planned schedule in advance, thus ensuring constant flexibility provision for a specified duration. The adopted case studies, which use a residential building and a local energy community, underpin the capabilities of the proposed framework and its applicability to energy systems with internal network constraints. One of the key findings is that the coupled flexibility from the heat vector significantly increases active power flexibility, i.e., the range of increase and decrease in its active power during operation. This anchors heat pumps as a linchpin coupling component between electricity and heat in MES. Furthermore, the interdependence between the maximum thermal output of the heat pump and the thermal capacity of the hot water storage tank was quantified by a linear threshold relation, beyond which increasing the size of the heat pump does not improve system flexibility.

1. Introduction

The path to carbon neutrality by 2050 depends on the transition of fossil-fuel-based energy systems to low-carbon energy systems. In turn, this is spearheaded by the increasing penetration of distributed energy resources (DER) [1]. Due to the variable nature of renewable DER and the growing electrification of other energy sectors such as heating and transport, flexibility in the electrical demand is crucial to ensuring a

* Corresponding author at: Forschungszentrum Jülich GmbH, Institute of Climate and Energy Systems, ICE-1: Energy Systems Engineering, Jülich 52425, Germany
Email addresses: p.gluecker@fz-juelich.de (P. Glücker), sleiman.mhanna@unimelb.edu.au (S. Mhanna), t.pesch@fz-juelich.de (T. Pesch), a.benigni@fz-juelich.de (A. Benigni), pierluigi.mancarella@unimelb.edu.au (P. Mancarella).

https://doi.org/10.1016/j.apenergy.2025.126342
Received 12 August 2024; Received in revised form 19 May 2025; Accepted 13 June 2025
Available online 26 June 2025

Nomenclature

Acronyms

BAT	Battery
COP	Coefficient of performance
ED	Electric demand
HD	Heat demand
HP	Heat pump
HWS	Hot water storage
LEC	Local energy community
MES	Multi-energy system
NOE	Nodal operating envelope
OP	Operating point
PCC	Point of common coupling
PV	Photovoltaic
SOC	State of charge
TAC	Total annualised cost

Design variables

$\overline{\dot{Q}}^{\mathrm{hp}}_{\mathrm{out}}$	Maximum thermal output power of heat pump
$C^{\mathrm{bat}}_{\mathrm{des}}$	Battery capacity
$C^{\mathrm{hws}}_{\mathrm{des}}$	Hot water storage capacity
$P^{\mathrm{pv}}_{\mathrm{nom}}$	Nominal active power output of PV array

Indices and set

τ, $\mathbb{D}$	Time step index for flexibility duration, set of flexibility time steps
c, $\mathcal{C}$	Component, set of all components
f, $\mathcal{F}$	Energy vector for flexibility calculation, set of energy vectors for flexibility calculation
i, $\mathcal{I}$	Storage component, set of storage components
s, $\mathbb{S}$	Scenario index, set of scenarios
t, $\mathbb{T}$	Time step index, set of time steps
v, $\mathcal{V}$	Energy vector, set of all energy vectors

Operational variables

$\dot{Q}^{r}_{\mathrm{in/out}}$	Heating power input/output of component r
b^{i}_{ch}	Binary charging variable of storage component i
$f^{\mathrm{pcc,ref}}_{s,\tau}$	Value for vector f at PCC for reference schedule at time (s,τ)
$f^{\mathrm{pcc}}_{s,\tau}$	Value for vector f at PCC at time (s,τ)
$f^{\mathrm{r}}_{s,\tau}$	Value for vector f of component r at time (s,τ)
$f^{\mathrm{down}\,\vert\,d}_{s,t}$	Downward flexibility for vector f at time (s,t) for duration d
$f^{\mathrm{flex}}_{s,t}$	Flexibility for vector f at time (s, τ)
$f^{\mathrm{up}\,\vert\,d}_{s,t}$	Upward flexibility for vector f at time (s,t) for duration d
$o_{\mathrm{s,t}}$	Operational variable value at time (s,t)
$P^{r}_{\mathrm{in/out}}$	Active power input/output of component r
$Q^{r}_{\mathrm{in/out}}$	Reactive power input/output of component r
$S^{r}_{\mathrm{in/out}}$	Apparent power input/output of component r

Parameters

Δt	Length of time step [h]
η^{pcc}	Electrical efficiency at PCC
η^{c}	Efficiency of component c
κ^{i}	Self-discharge time constant of storage i [1/h]
μ_{fix}	Annual fixed cost [%]
μ_{var}	Annual variable cost [€/kWh]
ψ	Response time of flexibility [h]
d	Duration of flexibility [h]
k_{ann}	Annualisation factor
r_{ik}	Resistance of line ik [Ω]
w_{s}	Weight of representative scenario day s
x_{ik}	Reactance of line ik [Ω]

reliable power supply [2–4]. In this context, an integrated analysis of multi-energy systems (MES) can unlock further potential to provide electrical flexibility [5,6]. Through the coupling of multiple energy vectors, MES can increase their flexibility and support power grid operation by offering several grid services, such as load shifting and demand response, proving that an integrated analysis of MES is essential for unlocking further flexibility [7–10].

There has been significant research in recent years regarding the operational flexibility of MES. In particular, a comprehensive overview of distributed multi-energy systems modelling and their flexibility applications is presented in [7], focusing on the role of multi-energy networks restricting or enabling flexibility. Another study demonstrates how an innovative multi-energy district can provide electrical flexibility to multiple services as demand response under uncertainty [11]. In addition, the real-time provision of electrical flexibility for a local energy community (LEC) is demonstrated in [9,12]. The LEC, supported by a community energy storage system, provides ancillary services to the wider power grid through the provision of load flexibility and the sharing of battery capacity in real-time. Moreover, integrating hydrogen into energy systems, for instance by injecting it into existing natural gas networks, enables further electrical flexibility for the power system, as electrolysers can be operated as flexible loads [13]. It is shown that although the gas network's operating conditions limit the overall flexibility contribution of electrolysers, power-to-gas units such as electrolysers can significantly increase power system flexibility. Similar to LECs, energy-intensive industrial process plants comprise multiple energy vectors, thus positioning them as MES that can provide flexibility. For instance, the demand-response flexibility of a cement production process can be utilised to minimise bid costs in sequential energy markets [14]. Another study proposes a flexibility assessment tool for industrial processes in [15], where feasible operating regions are quantified in terms of the potential of a given industrial process for the provision of grid services during operation. In another study, integrated flexible regions of an MES with process manufacturing are evaluated to provide flexibility during operation [16]. Moreover, multiple uncertainties concerning the flexibility provision of industrial parks are investigated, introducing probabilistic integrated flexible regions to describe the multi-energy adjustment capability of industrial parks [17].

Meanwhile, design and planning tools for MES focus on the economic part of their investment and the subsequent operation of the system. For instance, several revenue streams from participating in ancillary service markets for multi-energy microgrids are considered in [18], [19], significantly influencing the optimal sizing of resources. Similarly, multi-stage planning frameworks are proposed in [20] and [21] for industrial process plants, participating in frequency-balancing markets to create additional revenue, which in turn has an impact on new investments in process capacities for additional flexibility provision. In another study, the value of flexibility within a multi-energy production company is evaluated by providing flexibility services. These services include peak shaving, self-consumption optimisation and integrated demand response, thus contributing to decarbonisation and the reduction of costs [22]. All of the tools mentioned above focus on the economic part of the investment, which is partly driven by the price arbitrage of market participation. However, these tools do not provide technical insights into how operational flexibility is affected during the investment process, i.e., breaking down which components provide how much flexibility, the type of flexibility, the identification of interdependencies between

individual components and what would happen if the component sizes change.

While research has either explored the operational aspects of MES flexibility or has analysed the cost-optimised investment and operation, a knowledge gap exists in the flexibility consideration embedded in the design phase of MES. In particular, the influence of individual components on the electrical flexibility of MES has – to the best of our knowledge – not yet been explored. Here, the electrical flexibility provided by MES refers to the technical ability of the integrated system to dynamically adjust its electrical operating point by effectively utilising interconnected energy carriers. To bridge this gap, the presented work proposes a framework to quantify the impact of individual component design on the provision of operational flexibility by MES. More specifically, the framework identifies the key design components that enhance or hinder the provision of technical flexibility, thus merging the design aspect of MES with their capacity to provide flexibility during operation. An important aspect of this analysis involves a sensitivity analysis to quantify the precise impact of the design of each component on the overall flexibility of the whole system, and to identify interdependencies between individual components. Instead of relying solely on economic considerations, detailed technical insights and identified interdependencies between individual components provide a comprehensive understanding of system behaviour and identify key components that enable flexibility. By identifying critical components and their sensitivities, stakeholders can make more informed decisions when facing uncertainties, for instance concerning prices and demand forecasts.

Moreover, existing literature on flexibility typically considers only the transition from one operating point to another for a given duration and response time. However, this approach does not account for the relationship to subsequent time steps of a reference schedule, which is likely to differ from the current operating point due to, e.g., time-varying demand or variable photovoltaic (PV) irradiation. The pre-determined reference schedule is particularly important for large consumers such as virtual power plants (VPPs) or industrial process plants, which must submit their planned schedule one day in advance [23]. Therefore, it is crucial to consider the reference schedule when computing flexibility over multiple time steps. To address this gap, the presented framework calculates operational flexibility in relation to a predetermined reference schedule, thus accommodating constant flexibility offers for the specified duration. The proposed framework allows for a more comprehensive technical understanding of the electrical flexibility and the interactions between components within MES. The key contributions of this paper are as follows:

- Flexibility calculation over multiple time steps in relation to a predetermined reference schedule
- Technical assessment of electrical flexibility provision from MES embedded in the design stage
- Impact assessment of individual component design on overall system flexibility
- Sensitivity analysis to gain an understanding of interdependencies between components and identify thresholds regarding system flexibility, particularly for the heat pump as an energy vector-coupling component

The proposed framework is demonstrated on a residential building utilising electricity and heat as energy vectors, and a local energy community with several buildings including an internal power grid. These case studies serve as concrete examples for understanding the impact of component-level design on the provision of electrical flexibility and how the presented framework can offer valuable insights into the technical background of an MES providing flexibility in relation to a reference schedule. The rest of the paper is structured as follows: Section 2 describes the proposed methodology, followed by the presentation of the case study in Section 3. The case study results are provided and discussed in Section 4. Section 5 offers a conclusion to the study.

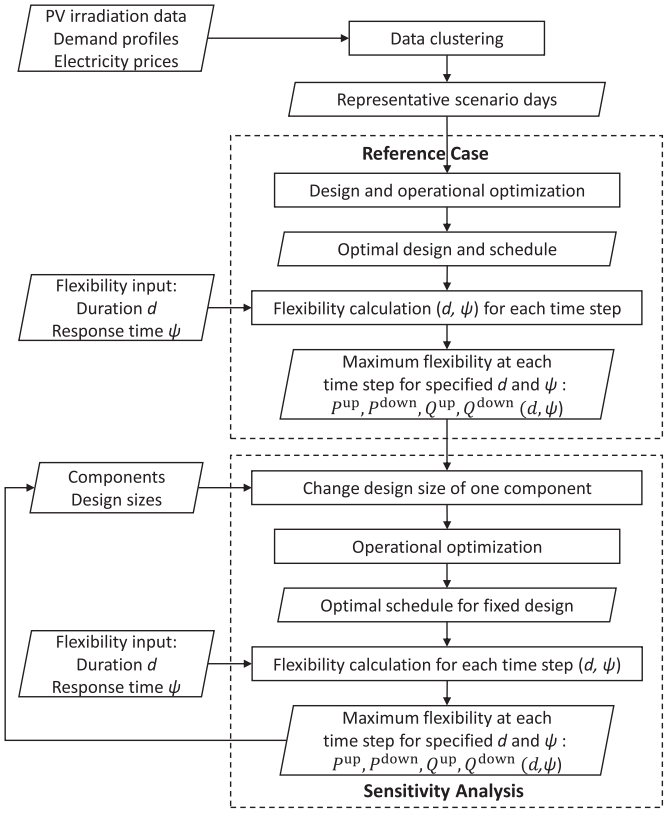

Fig. 1. Flowchart for the proposed algorithm.

2. Methodology

The suggested methodology builds on the optimisation-based nodal operating envelope (NOE) modelling framework for power systems, introduced in [24]. It further develops this approach by embedding the flexibility assessment in the design stage within MES and thus investigates the impact of component design. Moreover, this work addresses the provision of flexibility over multiple time steps in relation to the respective reference schedule of the MES, while also incorporating the intertemporal constraints of electrical and heat storage systems.

2.1. Integrated design and flexibility analysis framework

The proposed algorithm encompasses two main parts, as illustrated in Fig. 1, namely the reference case and the sensitivity analysis. During the pre-processing, the input data are clustered into representative scenario days. The first part of the reference case is the optimisation of the design and operation of the MES. Based on this schedule, the flexibility at each time step is computed, considering the specified flexibility duration and response time. The outcome includes the maximum achievable upward and downward flexibility for active and reactive power at the point of common coupling (PCC), respectively.

The second part of the proposed framework consists of a sensitivity analysis, iterating through varying design sizes for each component while keeping the remaining components at their reference size. Similar to the reference case, the flexibility for active and reactive power is calculated for each time step for the specified duration and response time, resulting in a time series with the maximum upward and downward flexibility for each time step. Note that this upward and downward flexibility relates to the previously optimised reference schedule at each time step. The details of the proposed methodology for the flexibility calculation for each time step are presented in Section (2.2). During post-processing, the maximum flexibility values for each time step during

the entire operation are subsequently aggregated, establishing a connection between design choice and the calculated flexibility range for a comprehensive analysis.

Furthermore, NOEs are calculated to visualise the operational flexibility at certain time steps. NOEs describe the time-varying active and reactive power limits during operation at the PCC where the MES can operate safely considering technical features such as response time, duration and network constraints [25]. A separate NOE is calculated for each time step. Based on [24], we vary the reactive power from its minimum to maximum values as a constraint at the PCC. For each reactive power value, the corresponding maximum and minimum active power are determined, resulting in a two-dimensional operating range that defines the limits for active and reactive power.

2.2. Flexibility calculation

As described in Section 2.1, the flexibility is calculated based on a previously determined design and optimal operation of the MES. In this study, flexibility is referred to as the technical ability to dynamically adjust the operating point by effectively utilising interconnected energy carriers. We define upward flexibility as the capability to increase the generation or decrease the consumption of the flexibility vector in relation to the reference schedule, while downward flexibility is defined vice versa. The inputs for the flexibility calculation are the response time ψ which is the time until the changing operating point must be reached, and the flexibility duration d which indicates the amount of time the deviation in operation must be provided for. Note that both upward and downward flexibility are assumed to be constant over the specified flexibility duration in relation to the reference schedule. Subject to the specified flexibility duration and response time, optimisations are performed at each time step for both upward and downward flexibility to quantify the system flexibility at the PCC. The flexibility is calculated during the reference case as well as for each iteration during the sensitivity analysis as depicted in Fig. 1. In the following, we introduce a generalised formulation for the flexibility vector, However, in the remaining paper, we assume that the flexibility vector is active power. Note that alternatively, one could use reactive power or heating power.

The upward flexibility for the flexibility vector f at each time step t of scenario day s is maximised as follows:

$$\max_{s\in\mathbb{S},t\in\mathbb{T}} \quad f_{s,t}^{\mathrm{up}\,|\,d} \tag{1a}$$

$$\text{s.t.} \quad f_{s,t}^{\mathrm{up}\,|\,d} \le f_{s,\tau}^{\mathrm{flex}}, \qquad \forall (s,t)\in(\mathbb{S},\mathbb{T}),\ \forall \tau\in\mathbb{D}(d), \tag{1b}$$

$$f_{s,\tau}^{\mathrm{flex}} = f_{s,\tau}^{\mathrm{pcc,ref}} - f_{s,\tau}^{\mathrm{pcc}}, \qquad \forall (s,t)\in(\mathbb{S},\mathbb{T}),\ \forall \tau\in\mathbb{D}(d), \tag{1c}$$

$$f_{s,\tau}^{\mathrm{pcc}} = \eta^{\mathrm{pcc}} \sum_{c\in C} f_{s,\tau}^{r}, \qquad \forall s\in\mathbb{S},\ \forall \tau\in\mathbb{D}(d), \tag{1d}$$

where $f\in\mathcal{F}=\{P,Q\}$ for electrical flexibility with $\mathcal{F}\subseteq\mathcal{V}$, d is the flexibility duration, with the time steps τ in $\mathbb{D}(d)\subseteq\mathbb{T}$ as the time steps for flexibility provision in the set $\mathbb{D}$, $\tau\in[t,t+1,\dots,t+n-1]$, and $f_{s,t}^{\mathrm{up}\,|\,d}$ and $f_{s,t}^{\mathrm{down}\,|\,d}$ represent the upward and downward provision of flexibility for the flexibility vector f over the flexibility duration of $n\cdot\Delta t$. Here, Δt is the time step size, $f_{s,\tau}^{\mathrm{pcc,ref}}$ is the energy vector value for the reference schedule and $f_{s,\tau}^{\mathrm{pcc}}$ is the variable vector at the PCC for scenario s at time instance τ, which is subject to the balancing-node constraint of the energy vector presented in (20) or the power flow equations presented in (21)–(26). The electrical efficiency at the PCC η^{pcc} accounting for electrical losses is included as part of the methodological approach. As the losses within buildings have a negligible impact on the system flexibility, the efficiency is assumed to be 1 within this work. Note the difference between the time instant t and the time instant τ; multiple instances of the latter (τ) must be considered for flexibility at the former (t), depending on the duration d. For instance, if the flexibility for one hour is determined at $t=30$, then $\tau\in\mathbb{D}=[30,31,32,33]$ for $d=1\,\mathrm{h}$ applies for $\Delta t=0.25\,\mathrm{h}$. For each time instant t, a new set of $\tau\in\mathbb{D}$ is formulated similarly. The objective function in (1a) maximises the upward flexibility. (1b) constraints the upward flexibility at time instant t as subject to the upward flexibility values at all time steps for which the flexibility should be determined, i.e., the maximum upward flexibility provision at the current time step t depends on the possible upward flexibility of each of the time steps τ during the duration d. (1c) defines upward flexibility as the difference between the reference schedule value which is fixed from the previously determined schedule optimisation, and the variable active power at the PCC, which is adjustable as a variable. The overall upward flexibility is then equal to the smallest maximum upward flexibility of all time steps during d. (1d) includes the balancing-node constraint of the flexibility vector considering an additional efficiency factor.

Downward flexibility, in contrast, can be formulated as:

$$\min_{s\in\mathbb{S},t\in\mathbb{T}} \quad f_{s,t}^{\mathrm{down}\,|\,d} \tag{2a}$$

$$\text{s.t.} \quad f_{s,t}^{\mathrm{down}\,|\,d} \ge f_{s,\tau}^{\mathrm{flex}}, \qquad \forall (s,t)\in(\mathbb{S},\mathbb{T}),\ \forall \tau\in\mathbb{D}(d), \tag{2b}$$

$$f_{s,\tau}^{\mathrm{flex}} = f_{s,\tau}^{\mathrm{pcc,ref}} - f_{s,\tau}^{\mathrm{pcc}}, \qquad \forall (s,t)\in(\mathbb{S},\mathbb{T}),\ \forall \tau\in\mathbb{D}(d), \tag{2c}$$

$$f_{s,\tau}^{\mathrm{pcc}} = \eta^{\mathrm{pcc}} \sum_{c\in C} f_{s,\tau}^{r}, \qquad \forall s\in\mathbb{S},\ \forall \tau\in\mathbb{D}(d). \tag{2d}$$

The difference in the calculation of the upward flexibility is that the downward flexibility is a negative value. Therefore, the downward flexibility in (2a) is minimised rather than maximised, and the less than or equal to sign in (2b) changes to a greater equality sign.

A graph showing the upward and downward active power flexibility across multiple time steps is depicted in Fig. 2, and serves to visualise (1) and (2) using the example of active power. The lines represent the reference active power schedule and the bar graphs show the upward and downward active power flexibility for a duration of four time steps. The provision of flexibility at the investigated time step t depends on the subsequent time steps τ for the flexibility duration. In this illustrated example, the PV array in Fig. 2 does not contribute upward active power flexibility due to the assumption that the active power generated by the PV array is fully dispatched. Only the electric battery (BAT) and the heat

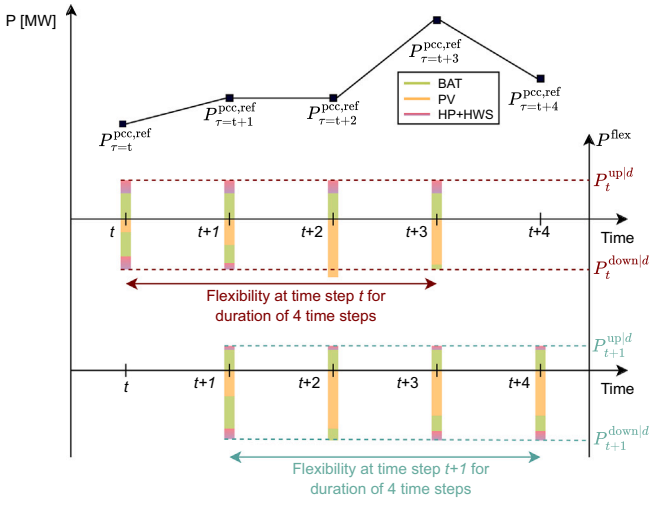

Fig. 2. Illustration of the flexibility calculation across multiple time steps using the example of active power. For a reference schedule, the bar graph shows the respective upward and downward active power flexibility at time step t and at time step $t+1$, respectively, for a duration of four time steps.

pump (HP) combined with the hot water storage (HWS) can provide upward active power flexibility. The overall upward flexibility is equal to the smallest maximum upward flexibility of all time steps during d as the flexibility provision is required to be constant. Depending on the predetermined reference schedule and the operation of each component, some time steps can offer more or less flexibility. Therefore, the optimisation shifts the active power provision of the existing storage systems to hours of the smallest maximum active power provision to maximise the overall maximum flexibility provision. This is especially evident in the downward flexibility, where possible PV curtailment at $\tau = t+2$ and $\tau = t+3$ allows for larger downward flexibility compared to $\tau = t$. Therefore, the battery is charged to increase its active power demand, while the HP increases its electricity consumption to charge the HWS, thus providing the majority of the downward flexibility across both storage systems at $\tau = t$.

2.3. Planning and operational modelling

This work adopts a component-oriented modelling approach, facilitating modular and scalable system design and operation, essential for MES. First, the energy component modelling in the case study under consideration is presented. Second, the objective function is described as used for the optimal design and operation of energy systems.

2.3.1. Component modelling

Storage components. For $i \in \mathcal{I} = \{\text{BAT}, \text{HWS}\}$: The governing equations for the electric battery and the hot water storage are as follows:

$$\begin{aligned}\text{SOC}^i_{t+1} = &\left(1 - \frac{1}{\kappa^i}\right)\text{SOC}^i_t \\ &+ \left(\eta^i_{\text{in}} P^i_{\text{in},t} - P^i_{\text{out},t}/\eta^i_{\text{out}}\right)\Delta t,\end{aligned} \tag{3}$$

$$\underline{E}^i \le \text{SOC}^i_t \le \overline{E}^i, \tag{4}$$

$$\underline{P}^i \le P^i_{\text{in},t} \le b^i_{\text{ch,t}} \cdot \overline{P}^i_t, \tag{5}$$

$$\underline{P}^i \le P^i_{\text{out},t} \le (1 - b^i_{\text{ch},t}) \cdot \overline{P}^i_t, \tag{6}$$

$$\overline{E}^i = C^i_{\text{des}}, \tag{7}$$

Here, SOC^i represents the state of charge of the storage system and κ^i denotes the self-discharge time constant per hour. The constant charging and discharging efficiencies $\eta^i_{\text{in/out}}$ are set at 0.95 for the BAT and 1 for the HWS. The charging and discharging power $P^i_{\text{in/out}}$ are constrained by upper and lower limits. The SOC is restricted by a lower limit $\underline{E}^i$ and an upper limit $\overline{E}^i$, with the latter being set as the storage capacity C^i_{des} design variable. For the HWS, we assume an ideal water storage without mixing effects and with perfect insulation [26], with an allowed temperature difference of 20 °C. The binary variable $b^i_{\text{ch,t}} \in [0, 1]$ ensures that the storage is not charged and discharged simultaneously, with $b^i_{\text{ch,t}} = 1$ indicating charging and $b^i_{\text{ch,t}} = 0$ indicating discharging.

Converter-based components. For $k \in \mathbb{K} = \{\text{BAT}, \text{PV}\}$: The electric battery and the PV panel are converter-connected devices and can therefore adjust their reactive power consumption/generation as follows:

$$S^{k2}_t = P^{k2}_t + Q^{k2}_t \le \overline{S^k}^2, \tag{8}$$

$$-\overline{S^k} \le Q^k_t \le \overline{S^k}, \tag{9}$$

$$\text{with} \quad P^k_t = P^k_{\text{in},t} - P^k_{\text{out},t}, \tag{10}$$

$$\text{and} \quad Q^k_t = Q^k_{\text{in},t} - Q^k_{\text{out},t}. \tag{11}$$

Here, S^k_t represents the apparent power of the component with the thermal limit of the converter $\overline{S^k}$, Q^k_t is the reactive power and P^k_t is the active power. For the PV panel $P^k_{\text{in},t} = 0 \,\forall\, t \in \mathbb{T}$ applies.

Photovoltaic array. The active power generation of the PV array is limited by the global tilted irradiance G of the sun, its efficiency η^{pv} and the total installed area A^{pv} as follows:

$$0 \le P^{\text{pv}}_t \le \eta^{\text{pv}} \cdot A^{\text{pv}} \cdot G, \tag{12}$$

$$P^{\text{pv}}_t \le P^{\text{pv}}_{\text{nom}}. \tag{13}$$

Heat pump. The HP model can represent air-to-water and water-to-water HPs by incorporating a variable coefficient of performance (COP) based on the temperature levels at the evaporator and the condenser. The governing equations are based on [27] and were adapted to the following:

$$\dot{Q}^{\text{hp}}_{\text{out},t} = COP^{\text{hp}}_t \cdot P^{\text{hp}}_t \tag{14}$$

$$\text{COP}^{\text{hp}}_t = COP_{\text{carnot},t} \cdot \eta^{\text{hp}}_{\text{sys}} \tag{15}$$

$$\text{COP}_{\text{carnot},t} = \frac{T^{\text{hp}}_{\text{out},t}}{T^{\text{hp}}_{\text{out},t} - T^{\text{hp}}_{\text{in},t}} \tag{16}$$

$$b^{\text{hp}}_{\text{op}} \underline{P}^{\text{hp}} \le P^{\text{hp}}_t \le b^{\text{hp}}_{\text{op}} \overline{P}^{\text{hp}}, \tag{17}$$

$$\dot{Q}^{\text{hp}}_{\text{out},t} \le \overline{\dot{Q}}^{\text{hp}}_{\text{out}}, \tag{18}$$

$$Q^{\text{hp}}_t = \tan(\varphi^{\text{hp}}) \cdot P^{\text{hp}}_t. \tag{19}$$

Here, P^{hp} represents the electric power input of the HP, which is limited by its lower part-load limit $\underline{P}^{\text{hp}}$ and its maximum output power $\overline{P}^{\text{hp}}$, $\dot{Q}^{\text{hp}}_{\text{out}}$ is the thermal output power which is limited by the design variable $\overline{\dot{Q}}^{\text{hp}}_{\text{out}}$. COP^{hp}_t represents the coefficient of performance of the heat pump, $\text{COP}_{\text{carnot},t}$ is the maximum theoretical COP of the Carnot process given the input temperature at the evaporator $T^{\text{hp}}_{\text{in},t}$ and the required output temperature at the condenser $T^{\text{hp}}_{\text{out},t}$. $\eta^{\text{hp}}_{\text{sys}}$ is the system efficiency which is assumed to be 0.5 and thus constant, as the part-load behaviour of the compressor of the HP does not have a large impact on planning studies and further lifts the computational burden [28]. The binary variable $b^{\text{hp}}_{\text{op}} \in [0, 1]$ indicates whether the heat pump is operating, thus ensuring the upper and lower power limit for $b^{\text{hp}}_{\text{op}} = 1$. Note that depending on the type of heat pump, $T^{\text{in}}_{\text{hp},t}$ is either the temperature of the low-temperature district heating (LTDH) network (water-to-water HP) or the ambient temperature (air-to-water HP). Furthermore, $T^{\text{hp}}_{\text{out},t}$ is equal to the input temperature requirement in the building, which is calculated based on the heat curve, with higher temperatures for lower ambient temperatures, and vice versa [29]. The reactive power consumption of the HP Q^{hp}_t depends on the active power consumption based on a constant power factor $\cos(\varphi^{\text{hp}})$.

The PQ flexibility capabilities of the presented components are depicted in Fig. 3. The battery is limited by its inverter rating, the PV array with its inverter is subject to its power factor limit of 0.9, and the HP has a constant inductive power factor of 0.9. It is assumed that the response time ψ for the battery and the PV array is a few seconds. The internal control of the HP's compressor from the manufacturer could limit

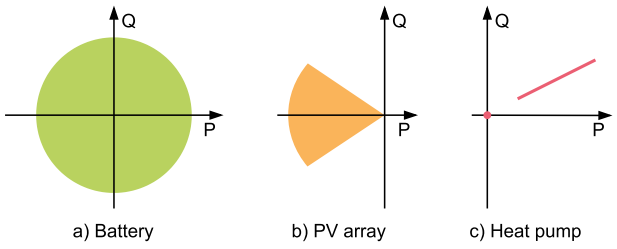

Fig. 3. Active power (P) and reactive power (Q) flexibility capabilities of the resources considered: battery, PV array, and heat pump. Note that positive values indicate consumption and negative values indicate generation.

the ramping of the HP [30], however, we assume a response time of a few minutes in this work. Therefore, the active and reactive power of all components can increase from minimum to maximum power values within the considered time step of 15 min and vice versa.

2.3.2. Energy vectors and power grid

The respective energy vectors of the components within the MES are connected and balanced. For each energy vector v in the set of vectors $\mathcal{V}$, balancing-node constraints balance the demand and generation of the respective vector for all components in the set C with a connector v^c associated with this energy vector, which is formulated as

$$\sum_{c \in C} v^c_{s,t} = 0, \quad \forall v \in \mathcal{V}, \quad \forall (s,t) \in (\mathbb{S}, \mathbb{T}), \tag{20}$$

where $\mathcal{V} = \{P, Q, \dot{Q}\}$, with P and Q representing active and reactive power, respectively, and $\dot{Q}$ representing the heating power. The import or export of active and reactive power for the energy vectors is included in each component.

Alternatively to balancing nodes, dedicated components can be created to represent energy networks and their underlying equations. The power grid is integrated based on the linear distribution flow (LinDistFlow) equations assuming a directed graph suitable for radial low-voltage and medium-voltage networks based on [31,32] as follows:

$$\sum_{k:i\to k} P_{ik,t} = P_{ji,t} + P_{i,t} \tag{21}$$

$$\sum_{k:i\to k} Q_{ik,t} = Q_{ji,t} + Q_{i,t}, \tag{22}$$

$$W_{k,t} = W_{i,t} - 2(r_{ik} P_{ik,t} + x_{ik} Q_{ik,t}), \tag{23}$$

$$(\underline{U}_k)^2 \le W_{k,t} \le (\overline{U}_k)^2, \tag{24}$$

$$|P_{ik,t}| + |Q_{ik,t}| \le \sqrt{2}\,\overline{S}_{ik}, \tag{25}$$

$$\left[|P_{ik,t}|, |Q_{ik,t}|\right] \le \left[\overline{S}_{ik}, \overline{S}_{ik}\right] \tag{26}$$

where k, i and j represent electric buses, P represents active, Q represents reactive, and S represents apparent power. W_k is an auxiliary operational variable defined as the square of the voltage magnitude U_k, r_{ik} is the line resistance and x_{ik} is the line reactance. The voltage drop across lines is integrated with (23), the voltage magnitude at each bus is kept within its limits by (24), while (25) and (26) constrain the active and reactive power flow across lines.

2.3.3. Objective function

For the reference case, the optimal design and operation of the MES are determined by minimising the total annualised cost (TAC). The TAC accounts for the initial investment cost (represented by i) of all components, as well as the annual fixed cost (fix) and variable operating cost (var). Subject to the balancing node constraints in (20) and the component characteristics given further below in (3)–(19), the objective function

$$C_i \cdot k_{\text{ann}} + \mu_{\text{fix}} \cdot C_i + \mu_{\text{var}} \sum_{s \in \mathbb{S}} w_s \sum_{t \in \mathbb{T}} o_{s,t} \Delta\tau \tag{27}$$

is to be minimised, where $\mathbb{S}$ is the set of scenario days, $\mathbb{T}$ is the set of time steps with a chosen duration of Δt in hours. w_s is a weighting factor that considers the distribution of days within each cluster, and k_{ann} is the annualisation factor which converts the investment cost into equal annual payments. Assuming a lifetime of 20 years and an interest rate of 6 %, the annualisation factor is approximately 0.087/a. The annual fixed cost μ_{fix} for maintenance depends on the overall investment cost C_i. The variable cost μ_{var} is associated with the operational parameter values $o_{s,t}$ which represents the operational parameter value for a given scenario day (s) and time interval (t), e.g., the value of active power or heating power. All the aforementioned parameters are component-specific as listed in Table 1 for the investigated case study. The term $o_{s,t}$ represents the operational parameter value for a given scenario day (s) and time interval (t) which has cost associated, e.g., the value of active power or heating power. For further details on the two-stage stochastic problem formulation, readers can refer to [33].

Table 1
Component parameter assumptions for the reference case.

Parameter	Battery	Heat pump	PV array	HWS
Lower limit	4 kWh	6 kW_{th}	4 kWp	8 kWh
Upper limit	10 kWh	15 kW_{th}	12 kWp	20 kWh
C_i	909 €/kWh	1300 €/kW_{th}	941 €/kWp	97 €/kWh
μ_{fix}	2.5 %	1.1 %	1.0 %	1.0 %
Sources	[34,35]	[35,36]	[34]	[35,37]

3. Case studies

Two case studies are presented to illustrate the capabilities of the framework. The first proposed case study represents a residential building with electricity and heat as depicted in Fig. 4. It consists of both electric demand (ED) and heat demand (HD), an electric battery, a PV panel, a heat pump, and a hot water storage. The selected case study is chosen due to the relevance of HPs as the key coupling element of MES within the residential sector. Due to their connected four-quadrant power converter, the PV array and the battery can provide both upward and downward reactive power flexibility, which depends on the active power setpoint, as depicted in Fig. 3. The thermal inertia of the building is not explicitly considered in this study due to the complexity of accurately estimating it in real-life cases and the limited availability of real-time measurements required to leverage inertia-based control strategies. The building is connected to the external power grid at the PCC with active power and reactive power, which are combined as electricity in the figure for reasons of simplicity.

The second case study represents a small local energy community that consists of three identical buildings, as depicted in Fig. 5. The goal of this case study is to highlight how the proposed approach can also be used for scenarios with an internal, relevant energy grid. The buildings are structured as in the first case study above, with all three buildings having identical components and parameters. The components of the same type are equally sized across the buildings. The LEC further includes an internal power grid that is connected to the external grid at the PCC via a transformer. Moreover, the water-to-water HPs are connected to an LTDH network. Due to its efficient pipe insulation, the temperature of the LTDH network is assumed to remain constant at 30 °C.

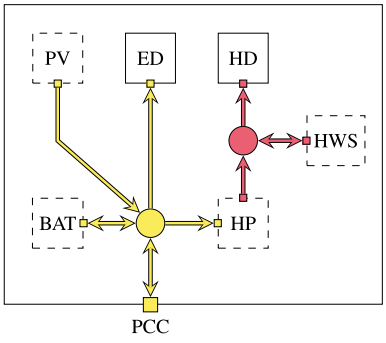

Fig. 4. Internal structure of the presented case study. The electric demand (ED) is met by the electricity connection of the building, the battery (BAT), and the photovoltaic (PV) panel. The heat pump (HP) supplies the heat demand (HD) and the hot water storage (HWS), which can also supply the heat demand. The red lines represent the hot water flow and the yellow lines represent the active power flow. The arrows of the lines indicate the energy carrier flow direction. The dashed-line components are to be sized.

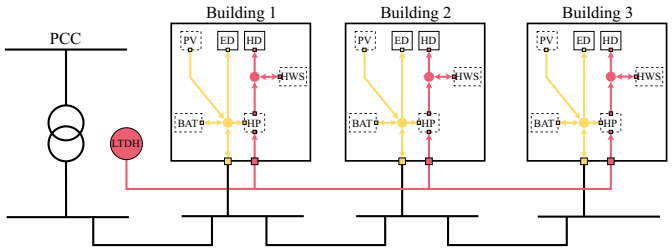

Fig. 5. Internal structure of the local energy community including an internal electricity grid and a low-temperature district heating (LTDH) network. Three buildings are connected by power cables at 400 V and the point of common coupling (PCC) is at 10 kV. The dashed-line components are to be sized. Note that components of the same type have the same size across all buildings.

For both case studies, the components depicted with dashed lines are to be designed within their respective limits listed in Table 1, which further lists the component-specific parameter values for the objective function. The variable operating cost for active power is assumed to be $\mu_{var} = 0.30$ €/kWh and the remuneration for selling active power at the PCC, i.e., feeding into the grid, is set to 0.05 €/kWh. For the LEC, the apparent power limit of the transformer is 40 kVA, while all cables have an apparent power limit of 32 kVA.

The input data for heat and electric demand are based on a residential apartment building taken from [38], whereas the data for the solar irradiation are taken from [39]. The given time series are clustered by means of k-medoids, which has proven to be effective in aggregating time-series data in energy systems [40]. The time step length is 15 min, and the electricity import and export prices are assumed to be constant.[1] The model and algorithm presented in Section 2 are implemented in the Python-based modelling framework COMANDO [33] and performed on a 1.8 GHz Intel Core i7-1265U CPU with 32 GB of RAM using Gurobi 10.0.1 [41].

4. Results

The results are presented in the following. Note that unless otherwise indicated, the analysed case study is the residential building equipped with a water-to-water heat pump. First, the operation of the reference schedule is analysed in Section 4.1. Second, the impact of the thermal vector is presented in Section 4.2. Third, the impact of an internal power grid is analysed using the example of the LEC in Section 4.3. Fourth, a sensitivity analysis regarding the individual component design is carried out and its results are analysed in Section 4.4. Subsequently, Section 4.5 presents the relationship between the heat pump and the hot water storage in depth.

4.1. Operational schedule for multi-energy system

An initial design and operational optimisation is carried out to determine the reference design and schedule of the residential building, with the optimal design parameters listed in Table 2. The operational schedule for the MES is depicted in Fig. 6 for all energy vectors. It can be seen that the first day represents a winter day with high HD and low PV generation, whereas the last day represents a summer day with low HD and high PV generation. The SOC of the BAT and HWS, depicted at the bottom of Fig. 6, are restricted to be at 50 % at the beginning and end of each representative day. This ensures that no energy is transferred between representative days.

[1] For the sake of highlighting the technical assessment of MES flexibility provision, we assume flat electricity prices, resulting in the minimisation of losses. However, the tool is capable of handling variable price signals, which would result in a more complex optimisation problem.

Table 2
Component sizes for the reference optimisation.

Component	Battery	Heat pump	PV array	HWS
Size	4 kWh	8.2 kW_{th}	12 kWp	10.8 kWh

The maximum and minimum possible values for both active power and reactive power at the PCC were calculated for each time step for a duration of 15 min. It is worth noting that the direction of flexibility is defined from the perspective of the external grid, i.e. upward flexibility indicates an increase in power generation or a decrease in consumption, while downward flexibility indicates a decrease in generation or an increase in consumption at the PCC. During periods of discharged battery and HWS (e.g. The first day), the MES operates at its minimum active power set point, thus limiting its ability to provide upward flexibility. Conversely, when solar PV generates excess power compared to internal demand, the battery and the HWS are charged, resulting in increased upward flexibility potential by discharging the battery or exploiting the thermal energy of the HWS instead of the HP to meet the HD.

4.2. Impact of thermal vector on electrical flexibility

Here, the impact of the thermal vector within the integrated MES on the electrical flexibility at the PCC is presented. Therefore, the integrated multi-energy reference case is compared to a similar system for which the HWS is removed, hereafter referred to as *electricity only* system. Within the electricity only system, the HP cannot operate flexibly but needs to meet the HD for each time step, thus only the PV array and the BAT can provide electrical flexibility.

The NOEs for three arbitrarily chosen time steps are depicted in Fig. 7 for two flexibility durations of 15 min and 60 min. As expected, the NOE area decreases as the flexibility duration d increases. Comparing the integrated multi-energy reference system with the case where the HWS is removed (electricity only), we observe a smaller NOE for the electricity only system compared to the integrated reference case for all three time steps and both flexibility durations. To quantify the difference in flexibility potential between the two systems, the maximum flexibility values for all time steps across the operational schedule can be aggregated, e.g., t_a, t_b and t_c in Fig. 6 result in one maximum upward and downward flexibility value, respectively. The mean maximum values for upward and downward active power flexibility over all time steps increase by 13.1 % for the integrated energy system compared to the electricity only system. This highlights the importance of integrated multi-energy flexibility assessment to understand the actual technical potential, and further emphasises the importance of coupling the heating sector with the electricity sector for increasing the electrical flexibility provision.

4.3. Impact of internal power grid

Here, the impact of the internal power grid within the second case study representing the LEC is analysed, which demonstrates the capabilities of the proposed framework to handle energy network constraints. For all buildings, the same input data as for the single residential building is used. As the power grid does not constrain the operation in the reference case, the components in each building are sized identically to the single residential building as listed in Table 2.

Fig. 8 illustrates how the increase in battery capacity influences both the operation and the NOE of the LEC for several time steps. It can be observed for $t_b = 346$, that different battery sizes can result in different operating points (OP) due to the newly optimised schedule for each design variation. Moreover, it can be seen that for $t_a = 48$, the maximum active power consumption is limited at 32 kW, which is reached for double the reference size of the battery. Despite increasing the battery capacity further, the maximum active power consumption cannot further increase. Similarly, for an increase and decrease of the reactive power consumption, the diagonal represents the apparent power limit

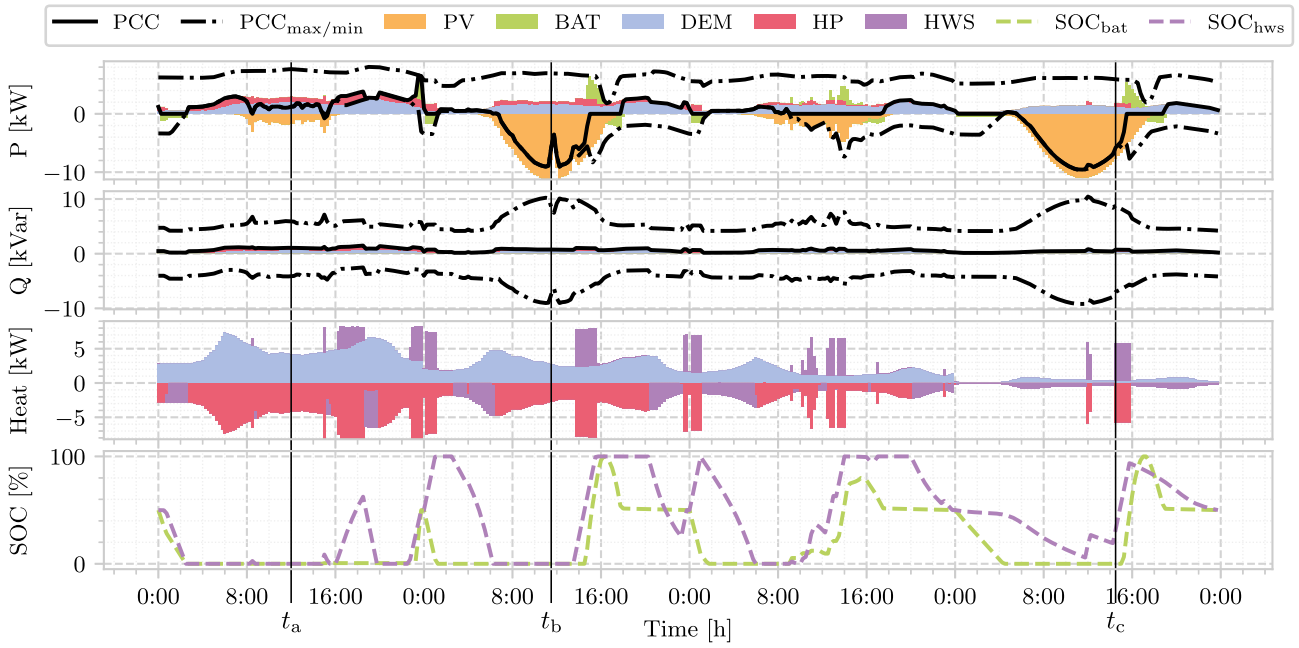

Fig. 6. Reference schedule of the residential building, with active power at the top, reactive power in the middle and heat at the bottom of the figure. Positive values correspond to consumption and negative values represent generation, while positive values for the PCC represent electricity import, and negative values for electricity export. $PCC_{max/min}$ represents the respective maximum and minimum active and reactive power values for the duration of 15 min. For conciseness, the electric demand (ED) – including both active and reactive power – and heat demand (HD) are referred to as demand (DEM).

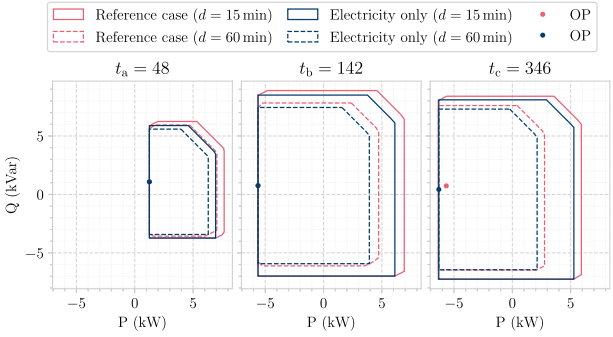

Fig. 7. Nodal operating envelope (NOE) and respective operating point (OP) of the overall system at three snapshot time steps t_a (Day 1, 12:00), t_b (Day 2, 11:30) and t_c (Day 3, 14:30) for the reference case and the only electricity system providing flexibility.

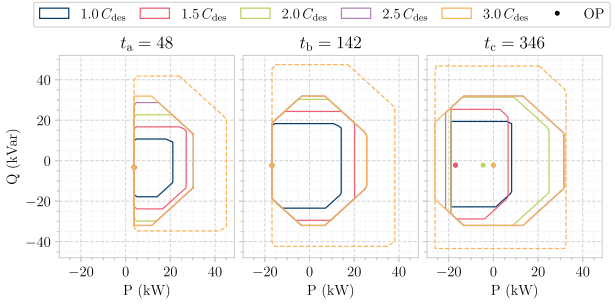

Fig. 8. Nodal operating envelope (NOE) for 60 min duration of the LEC at the PCC at three snapshot time steps t_a (Day 1, 12:00), t_b (Day 2, 11:30) and t_c (Day 3, 14:30) for design variations of the BAT in relation to its respective reference design C_{des}. The operating points (OP) refer to the NOE with the respective design size colour, and the dashed line represents the NOE without the internal power grid.

of the cables at 32 kVA. As a comparison, the dashed line represents the NOE without power grid constraints, which results in a significantly larger NOE compared to the NOE with the power grid. Fig. 8 clearly indicates the limiting effect of the underlying electricity network on the flexibility at the PCC due to apparent power limits or voltage magnitude limits.

4.4. Sensitivity analysis of individual component design

In the following, a sensitivity analysis of the individual component design is presented. To focus on a simple case study and better understand the sizing sensitivities and interdependencies between MES components, the residential building is considered as the case study for the remaining part of this study, i.e., no internal power grid is included.

To compare the overall flexibility capabilities of the MES for different individual component designs, the maximum flexibility values for all time steps across the operational schedule are aggregated within one data set. The given setup with four representative days and 15 min time steps results in 384 flexibility values for a given design. These values can be visualised in a box plot to quantify and compare the distribution and average upward and downward flexibility values of different component designs. This is depicted in Fig. 9 for different component sizes of the PV array, providing insights into the impact of component sizing on overall system flexibility. For each box plot with the accompanying different PV array size, a cost-optimal reference schedule is determined, and for each time step the maximum upward and downward flexibility is calculated depending on the desired flexibility duration. With an increasing PV size (while other components remain at their reference size), the downward flexibility P_{down} increases significantly due to the higher curtailment potential, while the upward flexibility P_{up} remains relatively constant. The widening interquartile range and the increase in outliers for downward flexibility with increasing PV sizes indicate a broader distribution of the maximum downward flexibility. This can be explained by the limited availability of active power PV generation, which is only available during hours of solar irradiation. During these

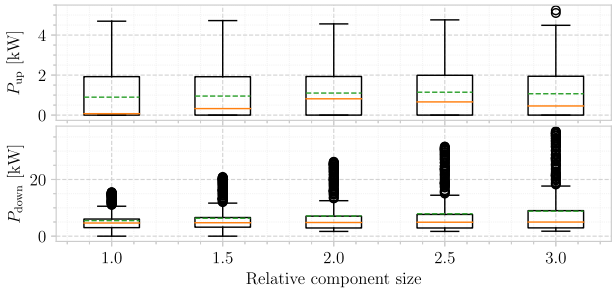

Fig. 9. Maximum active power flexibility (60 min duration) of the overall MES depending on the design variation for the PV array relative to its reference design. The green dashed lines represent the mean and the orange lines represent the median of the data set.

times, a larger PV panel can provide significant flexibility from curtailment. In contrast, during hours when there is no solar irradiation, the PV array is unable to provide active power flexibility. The mean values as shown in Fig. 9 for upward flexibility P_{up} and downward flexibility P_{down} for a single variation of each component are shown in Fig. 10. A new operational optimisation is performed for each design combination (see Fig. 1). The resulting different schedules are the reason why an increasing size results in decreasing upward flexibility for some components. However, the corresponding larger increase in downward flexibility results in an overall increased NOE. Furthermore, it can be observed that increasing the size of the HP individually does not change its flexibility above its relative size of 1.5, which can be attributed to the interdependence between the HP and HWS, where the fixed size of the other restricts the size of one component. The thermal inertia of the building is not explicitly modelled, which means that the HP cannot operate flexibly on its own, as it must meet the predetermined inflexible heat demand of the building. A combined approach was therefore adopted to overcome this identified constraint and to assess the system flexibility for these components, increasing both the HWS and HP sizes simultaneously and resulting in increasing downward flexibility as shown in the right column of the figure.

The additional investment cost and total annualised cost per unit in relation to the reference case are shown in Fig. 11. It can be seen that due to the low investment cost of the HWS, increasing its size along with the HP increases the mean active power flexibility provision of the overall system significantly.

To assess the difference between air-to-water HP and water-to-water HP in terms of electrical flexibility provision, Fig. 12 depicts the mean

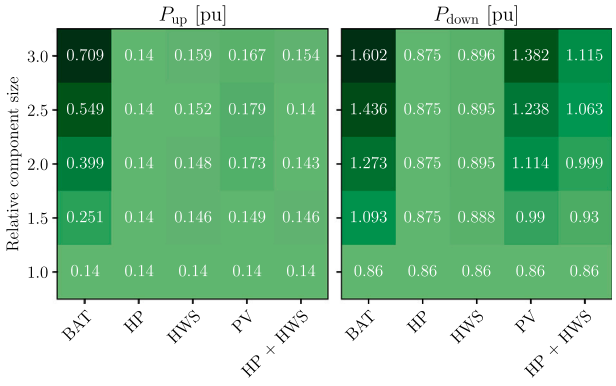

Fig. 10. Mean of maximum active power flexibility values (60 min duration) of the overall MES in relation to the reference case varying one component at a time. The flexibility per unit refers to the sum of the means for upward and downward flexibility in the reference case.

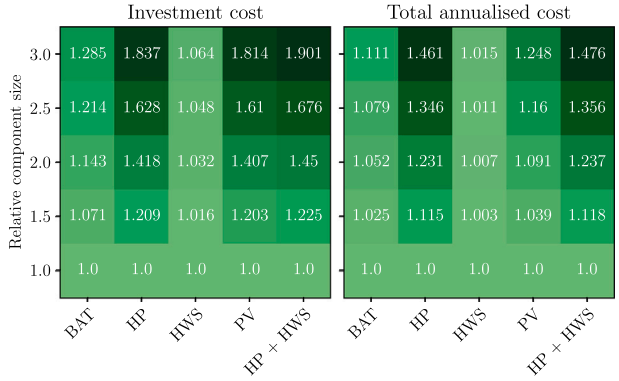

Fig. 11. Investment cost and total annualised cost of the overall MES in relation to the respective cost for the reference case. The total annualised cost does not include any remuneration for flexibility provision.

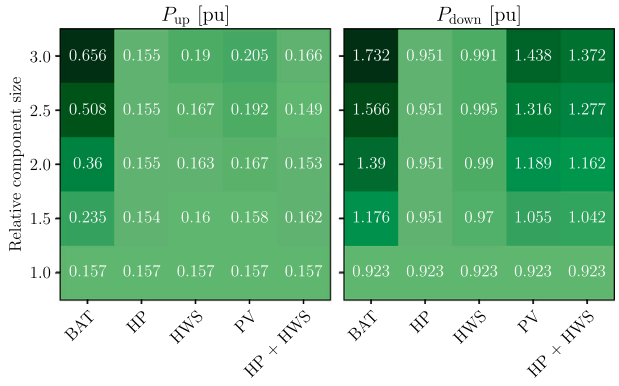

Fig. 12. Mean of maximum active power flexibility values (60 min duration) of the overall MES in relation to the reference case varying one component at a time for the air-to-water heat pump. The flexibility per unit refers to the sum of the means for upward and downward flexibility in the reference case with the water-to-water heat pump.

values for upward and downward flexibility for individual component variations. Note that per-unit values refer to the flexibility of the energy system with the water-to-water HP. Furthermore, the component sizes of this system are identical to the system with the water-to-water HP. For the reference case with relative component sizes of one, both upward and downward flexibility values are higher than those of the water-to-water HP depicted in Fig. 10, with a combined increase of 9.0 %. Moreover, a combined increase in air-to-water HP and HWS further amplifies the difference in active power flexibility provision between air-to-water and water-to-water HPs. The main reason for the larger electrical flexibility potential lies in the lower COP and thus the higher electricity consumption of the air-to-water HP due to the lower temperature at the evaporator.

4.5. Interdependency between heat pump and hot water storage

In addition to the individual analysis of each component, we explore the interdependencies influencing the provision of flexibility within the MES by varying two components at a time. Fig. 13 shows the mean values for upward and downward flexibility when varying two components at a time for the HP and HWS. As shown above, increasing the size of the HP alone above its relative size of 150 % does not increase the flexibility potential of the MES. However, as the size of the HWS is increased, there is an initial increase in flexibility with the subsequent increases in the size of the HP. Beyond a certain threshold of the HP size, flexibility

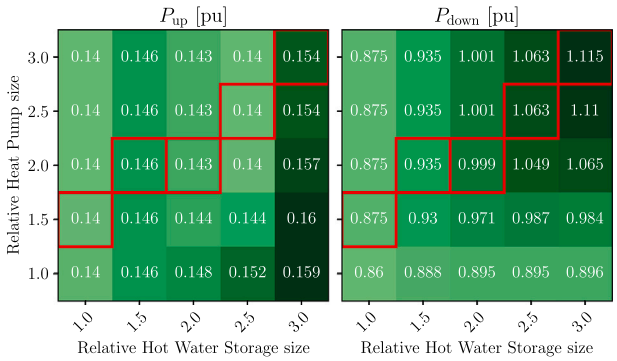

Fig. 13. Mean of maximum active power flexibility values (60 min duration) of the overall MES in relation to the reference case when varying two components at a time for the heat pump (HP) and hot water storage (HWS). The red boxes indicate the maximum mean flexibility values for a given HWS size.

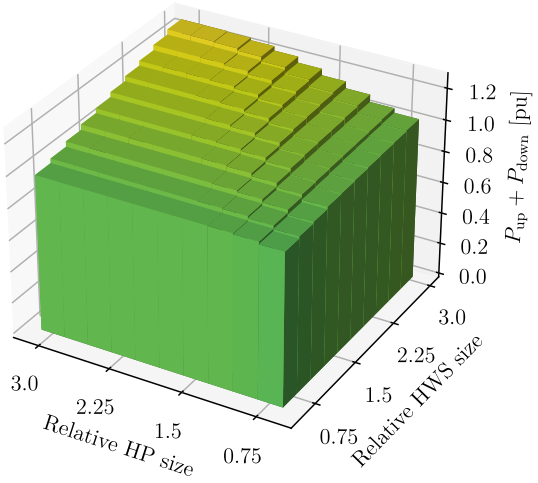

Fig. 14. Mean of maximum active power flexibility values (60 min duration) of the overall MES in relation to the reference case when varying two components at a time for the heat pump (HP) and hot water storage (HWS). The flexibility per unit refers to the sum of the means for upward and downward flexibility in the reference case.

reaches a plateau, indicating that further investment in a larger HP without increasing the size of the HWS will not result in greater flexibility. This threshold can be identified as the ratio of the maximum thermal output power of the HP $\overline{\dot{Q}}^{\text{hp}}_{\text{out}}$ to the thermal capacity of the HWS $C^{\text{hws}}_{\text{des}}$. It can be seen from Fig. 13 that – for the given case study – both the upper and lower active power flexibility remain unchanged with an increase in HP size above the relative ratio of 1.5. These values are highlighted by the red boxes, indicating that increasing the HP size while keeping the size of the HWS unchanged, i.e., moving up in each column, does not increase the upper or the lower flexibility. By using the component sizes from the reference optimisation in Table 2, and applying linear regression to the identified threshold values indicated by the red boxes, the linear relation for the threshold maximum thermal output power of the HP $\overline{\dot{Q}}^{\text{hp}}_{\text{out, TH}}$, given the thermal capacity of the HWS, is as follows:

$$\overline{\dot{Q}}^{\text{hp}}_{\text{out, TH}} = 5.89 + 0.56\, C^{\text{hws}}_{\text{des}}\ [\text{kW}_{\text{th}}].$$

Increasing the size of the HP above this threshold will therefore not result in any gain in flexibility, which means that investments should be made in a larger HWS. For instance, for the given case study, if the HWS size is 27 kWh, then an HP with a maximum thermal output larger than 20.5 kW_{th} does not increase the flexibility of the overall system. This can be seen in the reference case where for a relative HWS size of 2.5, an increase of the HP above 20.5 kW_{th} does not result in any improvement in system flexibility. These findings highlight the importance of the energy storage capabilities of heat pumps in improving flexibility within MES.

For a more detailed visualisation, Fig. 14 depicts the total active power flexibility, i.e., the sum of the mean upward flexibility P_{up} and the downward flexibility P_{down}, with a higher level of granularity. It further emphasises the impact of the HWS size on the improvement in overall flexibility by clearly visualising the plateaus for a fixed HWS size, above which an increase in HP size does not lead to any improvement in flexibility, thus underlining the importance of the energy storage capabilities of heat pumps when it comes to flexibility considerations.

5. Conclusion

This study presents a technical framework for quantifying the impact of component design choices on providing flexibility in multi-energy systems during their design phase. The framework identifies key components that enable or reduce flexibility. Furthermore, it allows for a quantified flexibility analysis over multiple time steps that is dependent on a predetermined reference schedule while considering different durations of flexibility. Two case studies underpin the capabilities of the proposed framework and provide valuable insights into electrical flexibility provision by local multi-energy systems. It was shown that integrating the heat vector significantly increases the electrical flexibility potential of multi-energy systems. Moreover, the impact of each component's size on the overall flexibility of the system is analysed and quantified, and interdependencies between components are identified. The presented framework enables a deeper technical understanding of the complex multi-energy interdependencies between components, including network constraints.

However, several assumptions in this study might limit its findings. First, assuming a constant COP may overestimate the efficiency of the HP under part-load conditions, thus potentially affecting its flexibility provision. Second, the HP might not be able to fully ramp up or down within 15 min, which would also reduce its flexibility. Future work could address these issues by integrating a variable COP and adding ramping constraints, which could be implemented with minimal modification in the presented framework. Third, the quantity and quality of the chosen representative days may influence the estimated flexibility, and thus should be selected carefully. Finally, the local energy community consists of identical buildings. Future studies could apply the framework to more diverse energy communities with varying household types or to complex multi-energy systems such as industrial process plants that integrate additional energy vectors, e.g., gas. Furthermore, co-optimising the component sizing and the flexibility provision by integrating economic flexibility markets is the subject of ongoing work. These advances will help contribute to a more comprehensive understanding of how planning decisions affect the electrical flexibility of multi-energy systems and vice versa, which could guide investment decision processes within MES offering flexibility services.

CRediT authorship contribution statement

Philipp Glücker: Conceptualization, Data curation, Investigation, Methodology, Software, Validation, Visualisation, Writing – Original Draft, Writing - Review and Editing. **Sleiman Mhanna:** Conceptualization, Validation, Writing – Review and Editing, Supervision. **Thiemo Pesch:** Funding acquisition, Supervision, Writing – Review and Editing. **Andrea Benigni:** Funding acquisition, Supervision, Writing – Review and Editing. **Pierluigi Mancarella:** Conceptualisation, Supervision, Writing – Review and Editing.

Declaration of competing interest

The authors declare that they have no known competing financial interests or personal relationships that could have appeared to influence the work reported in this paper.

Acknowledgements

PG would like to thank the Jülich-University of Melbourne Postgraduate Academy (JUMPA) for the scholarship provided, and the Helmholtz Association of German Research Centres for programme-oriented funding through the Innovation Pool project “Energiewende und Kreislaufwirtschaft” (energy transition and circular economy).

Data availability

Data will be made available on request.

References

[1] IPCC. Climate change 2023: synthesis report. contribution of working groups I, II and III to the sixth assessment report of the intergovernmental panel on climate change [core writing team.H. Lee and J. Romero (eds.)] *Geneva, Switzerland IPCC*; 2023, p. 35–115.
[2] Rinaldi A, Soini MC, Streicher K, Patel MK, Parra D. Decarbonising heat with optimal PV and storage investments: a detailed sector coupling modelling framework with flexible heat pump operation. Appl Energy 2021;282:116110.
[3] Bistline JET, Roney CW, McCollum DL, Blanford GJ. Deep decarbonization impacts on electric load shapes and peak demand. Environ Res Lett 2021 Sep;16(9):094054.
[4] Akrami A, Doostizadeh M, Aminifar F. Power system flexibility: an overview of emergence to evolution. J Mod Power Syst Clean Energy 2019;7(5):987–1007.
[5] Mancarella P. MES (multi-energy systems): an overview of concepts and evaluation models. Energy 2014 Feb;65:1–17.
[6] Enescu D, Chicco G, Porumb R, Seritan G. Thermal energy storage for grid applications: current status and emerging trends. Energies 2020;13(2):340.
[7] Chicco G, Riaz S, Mazza A, Mancarella P. Flexibility from distributed multienergy systems. In: Proc IEEE 2020; Sep. 2020. vol. 108 no. (9): 1496–517.
[8] Glücker P, Pesch T, Benigni A. Optimal sizing of battery energy storage system for local multi-energy systems: the impact of the thermal vector. Appl Energy 2024;372:123732.
[9] Avramidis I-I, Nagpal H, Mehrtash M, Capitanescu F. gEnesis: design, operation and integration of smart sustainable buildings in smart power grids. In: 2021 29th Mediterranean conference on control and automation (MED); 2021. p. 45–52, 2473-3504.
[10] Nagpal H, Avramidis I-I, Capitanescu F, Madureira AG. Local energy communities in service of sustainability and grid flexibility provision: hierarchical management of shared energy storage. IEEE Trans Sustain Energy 2022;13(3):1523–35.
[11] Good N, Mancarella P. Flexibility in multi-energy communities with electrical and thermal storage: a stochastic, robust approach for multi-service demand response. IEEE Trans Smart Grid 2019;10(1):503–13.
[12] Avramidis I-I, Capitanescu F, Deconinck G, Nagpal H, Heiselberg P, Madureira A. From the humble building to the smart sustainable grid: empowering consumers, nurturing bottom-up electricity markets, and building collaborative power systems. IEEE Power Energy Mag 2023;21(4):53–63.
[13] De Corato A, Saedi I, Riaz S, Mancarella P. Aggregated flexibility from multiple power-to-gas units in integrated electricity-gas-hydrogen distribution systems. Electr Power Syst Res 2022;212:108409.
[14] Bohlayer M, Fleschutz M, Braun M, Zöttl G. Energy-intense production-inventory planning with participation in sequential energy markets. Appl Energy 2020;258:113954.
[15] Ledur S, Molinier R, Sossan F, Alais J-C, Faris M-DEA, Kariniotakis G. Identification and quantification of the flexibility potential of a complex industrial process for ancillary services provision. Electr Power Syst Res 2022;212:108396.
[16] Hui H, Bao M, Ding Y, Song Y. Exploring the integrated flexible region of distributed multi-energy systems with process industry. Appl Energy 2022;311:118590.
[17] Hui H, Bao M, Ding Y, Yan J, Song Y. Probabilistic integrated flexible regions of multi-energy industrial parks: conceptualization and characterization. Appl Energy 2023;349:121521.
[18] Cardoso G, Stadler M, Mashayekh S, Hartvigsson E. The impact of ancillary services in optimal der investment decisions. Energy 2017;130:99–112.
[19] Contreras SF, Cortes CA, Myrzik JM. Multi-objective probabilistic power resources planning for microgrids with ancillary services capacity. In: 2018 power systems computation conference (PSCC); 2018. p. 1–8.
[20] Nolzen N, Leenders L, Bardow A. Flexibility-expansion planning for enhanced balancing-power market participation of decentralized energy systems, In: Computer aided chemical engineering. vol. 50. Elsevier; 2021. p. 1841–46.
[21] Richstein JC, Hosseinioun SS. Industrial demand response: how network tariffs and regulation (do not) impact flexibility provision in electricity markets and reserves. Appl Energy 2020;278:115431.
[22] Fleschutz M, Bohlayer M, Braun M, Murphy MD. From prosumer to flexumer: case study on the value of flexibility in decarbonizing the multi-energy system of a manufacturing company. Appl Energy 2023;347:121430.
[23] Next Kraftwerke. Was ist Ausgleichsenergie? 2024. [Online]. Available: https://www.next-kraftwerke.de/wissen/ausgleichsenergie. [Accessed on 10/07/2024].
[24] Riaz S, Mancarella P. Modelling and characterisation of flexibility from distributed energy resources. IEEE Trans Power Syst 2022;37(1):38–50.
[25] Liu MZ, Ochoa LF, Wong PKC, Theunissen J. Using opf-based operating envelopes to facilitate residential der services. IEEE Trans Smart Grid 2022;13(6):4494–504.
[26] Liu D, Carta D, Xhonneux A, Müller D, Benigni A. Short-term control of heat pumps to support power grid operation. In: EEE Open J Ind Electron Soc 2024: 1–18.
[27] Sass S, et al. Model compendium, data, and optimization benchmarks for sector-coupled energy systems. Comput Chem Eng 2020;135:106760.
[28] Glücker P, Mhanna S, Pesch T, Benigni A, Mancarella P. Electrical storage design in multi-energy systems: impact of component model choice. In: 2024 IEEE PES Innovative Smart Grid Technologies Europe (ISGT EUROPE); 2024. p. 1–5.
[29] Hering D, Cansev ME, Tamassia E, Xhonneux A, Müller D. Temperature control of a low-temperature district heating network with model predictive control and mixed-integer quadratically constrained programming. Energy 2021;224:120140.
[30] Evens M, Arteconi A. Design energy flexibility within a comfort and climate box – an experimental evaluation of the internal heat pump control effects. Appl Therm Eng 2024;254:123842.
[31] Low SH. Convex relaxation of optimal power flow—Part I: Formulations and equivalence. IEEE Trans Control Netw Syst 2014;1(1):15–27.
[32] Naughton JC. A modelling framework for virtual power plants under uncertainty, [PhD thesis], University of Birmingham; 2022.
[33] Langiu M, et al. Comando: a next-generation open-source framework for energy systems optimization. Comput Chem Eng 2021;152:107366.
[34] Graham P, Hayward J, Foster J. GenCost 2023-24: final report. Tech. Rep CSIRO; 2024.
[35] Baumgärtner N, Delorme R, Hennen M, Bardow A. Design of low-carbon utility systems: exploiting time-dependent grid emissions for climate-friendly demand-side management. Appl Energy 2019;247:755–65.
[36] Hering D, Xhonneux A, Müller D. Design optimization of a heating network with multiple heat pumps using mixed integer quadratically constrained programming. Energy 2021;226:120384.
[37] Ofenseite. Pufferspeicher 500. [Online]. Available: https://www.ofenseite.com/6100108-pufferspeicher-500 [Accessed on 31/10/2024].
[38] Npro - district energy planning tool, [Online]. Available: https://www.npro.energy [Accessed on 2/08/2023].
[39] Solcast. Global solar irradiance data and pv system power output data. [Online]. Available: https://solcast.com/ [Accessed on 2019 2/08/2023].
[40] Schütz T, Schraven MH, Fuchs M, Remmen P, Müller D. Comparison of clustering algorithms for the selection of typical demand days for energy system synthesis. Renew Energy 2018;129:570–82.
[41] Gurobi Optimization LLC. Gurobi optimizer reference manual. 2023. [Online]. Available: https://www.gurobi.com